



OPEN ACCESS

EDITED BY

Nian Wang,
Indiana University School of Medicine,
United States

REVIEWED BY

Hongda Shao,
Shanghai Jiao Tong University, China
Alfonso Mastropietro,
Istituto di Tecnologie Biomediche—Consiglio
Nazionale delle Ricerche, Italy

*CORRESPONDENCE

Yajun Ma
✉ yam013@ucsd.edu

[†]These authors have contributed equally
to this work and share first authorship

RECEIVED 19 July 2023

ACCEPTED 18 September 2023

PUBLISHED 28 September 2023

CITATION

Shaterian Mohammadi H, Moazamian D,
Athertya JS, Shin SH, Lo J, Suprana A, Malhi BS
and Ma Y (2023) Quantitative myelin water
imaging using short TR adiabatic inversion
recovery prepared echo-planar imaging
(STAIR-EPI) sequence.
Front. Radiol. 3:1263491.
doi: 10.3389/fradi.2023.1263491

COPYRIGHT

© 2023 Shaterian Mohammadi, Moazamian,
Athertya, Shin, Lo, Suprana, Malhi and Ma. This
is an open-access article distributed under the
terms of the [Creative Commons Attribution
License \(CC BY\)](https://creativecommons.org/licenses/by/4.0/). The use, distribution or
reproduction in other forums is permitted,
provided the original author(s) and the
copyright owner(s) are credited and that the
original publication in this journal is cited, in
accordance with accepted academic practice.
No use, distribution or reproduction is
permitted which does not comply with these
terms.

Quantitative myelin water imaging using short TR adiabatic inversion recovery prepared echo-planar imaging (STAIR-EPI) sequence

Hamidreza Shaterian Mohammadi[†], Dina Moazamian[†],
Jiyo S. Athertya, Soo Hyun Shin, James Lo, Arya Suprana,
Bhavsimran S. Malhi and Yajun Ma^{*}

Department of Radiology, University of California San Diego, San Diego, CA, United States

Introduction: Numerous techniques for myelin water imaging (MWI) have been devised to specifically assess alterations in myelin. The biomarker employed to measure changes in myelin content is known as the myelin water fraction (MWF). The short TR adiabatic inversion recovery (STAIR) sequence has recently been identified as a highly effective method for calculating MWF. The purpose of this study is to develop a new clinical transitional myelin water imaging (MWI) technique that combines STAIR preparation and echo-planar imaging (EPI) (STAIR-EPI) sequence for data acquisition.

Methods: Myelin water (MW) in the brain has shorter T_1 and T_2 relaxation times than intracellular and extracellular water. In the proposed STAIR-EPI sequence, a short TR (e.g., ≤ 300 ms) together with an optimized inversion time enable robust long T_1 water suppression with a wide range of T_1 values [i.e., (600, 2,000) ms]. The EPI allows fast data acquisition of the remaining MW signals. Seven healthy volunteers and seven patients with multiple sclerosis (MS) were recruited and scanned in this study. The apparent myelin water fraction (aMWF), defined as the signal ratio of MW to total water, was measured in the lesions and normal-appearing white matter (NAWM) in MS patients and compared with those measured in the normal white matter (NWM) in healthy volunteers.

Results: As seen in the STAIR-EPI images acquired from MS patients, the MS lesions show lower signal intensities than NAWM do. The aMWF measurements for both MS lesions ($3.6 \pm 1.3\%$) and NAWM ($8.6 \pm 1.2\%$) in MS patients are significantly lower than NWM ($10 \pm 1.3\%$) in healthy volunteers ($P < 0.001$).

Discussion: The proposed STAIR-EPI technique, which can be implemented in MRI scanners from all vendors, is able to detect myelin loss in both MS lesions and NAWM in MS patients.

KEYWORDS

myelin water imaging, STAIR, EPI, multiple sclerosis, aMWF

1. Introduction

Myelin is a lipid-protein bilayer that surrounds the axonal fibers of neurons (1). It plays an essential role in normal brain function by facilitating the rapid conduction of action potentials in the axon (2). Many neurological and degenerative diseases, such as multiple sclerosis (MS), are characterized by myelin damage and loss (3, 4). Thus, evaluations of demyelination and remyelination are essential for the accurate diagnosis and treatment monitoring of these diseases. Conventional magnetic resonance imaging (MRI) techniques, such as T_1 - and T_2 -weighted fast spin echo (T_1 w- and T_2 w-FSE), provide high

soft-tissue contrast and are routinely used in the diagnosis of MS and many other neurological diseases. However, these clinical sequences are unable to distinguish demyelination lesions, such as those observed in MS, from the ones caused by inflammation, edema, axonal loss, or gliosis (5–7). Moreover, it is also difficult for clinical MRI to detect myelin damage in brains that appear to be normal (i.e., where there are no apparent lesions) (8). Consequently, developing myelin-specific imaging techniques is of critical importance to improved evaluation of neurological diseases in clinical practice.

In the last two decades, many myelin water imaging (MWI) techniques have been developed for the specific evaluation of myelin changes. Myelin water (MW) is the water component tightly bound or trapped in the myelin bilayer (9–14). It has much shorter T_1 and T_2 relaxation times than intracellular/extracellular water. Myelin water fraction (MWF), defined as the signal ratio of MW to total water, is the biomarker used to quantify MW content changes (15–18).

State-of-the-art MWI techniques like multi-echo spin echo T_2 relaxometry (15), multicompartment analysis of T_2^* decay (16), and multicomponent-driven equilibrium single-pulse observation of T_1 and T_2 (mcDESPOIT) (17) have been developed to quantify MWF and have been applied for the assessment of MS. The high correlation between the MRI-measured MWF and histologically quantified myelin content has been demonstrated in brain sample studies (19, 20). Moreover, all these techniques are able to detect significant MWF decreases in demyelinated lesions in patients with MS in comparison to the normal white matter (NMW) in healthy individuals (15–17, 21, 22). Despite the success of these myelin-specific techniques, studies have found that these multicompartment modeling techniques are sensitive to system flaws such as B_1 and B_0 inhomogeneities (23–27). Different data post-processing strategies may also produce different results (28–31). Consequently, these techniques suffer from limited accuracy and robustness in terms of MWF estimation, shortcomings that slow down their clinical translation.

Another promising technique that has been developed for selective imaging of MW, known as direct visualization of short transverse relaxation time component (ViSTa), is based on the T_1 difference between MW and long T_2 intracellular/extracellular water components (32). The T_1 relaxation times for the long T_2 components in white matter and gray matter range from 750 to 1,000 ms and from 1,300 to 1,800 ms, respectively, at 3T (32–34). In contrast, the T_1 relaxation times for MW components are typically shorter than 600 ms (17, 18, 35, 36). This technique employs a double inversion recovery (DIR) preparation to robustly suppress all the long T_1 water components in the brain. Moreover, not only is ViSTa less sensitive to B_1 and B_0 inhomogeneities, but it does not require any complicated modeling to quantify MWF. That being said, ViSTa's scan time is too long for clinical use for whole brain coverage (~3 min per slice).

Most recently, Ma et al. have developed a short TR adiabatic inversion recovery (STAIR) technique in combination with a 3D Cones acquisition (STAIR-Cones) for time-efficient selective MWI in the whole brain (37). This technique uses a short TR to

suppress long T_1 water components with a variety of T_1 s. Similar to ViSTa, the STAIR sequence is relatively insensitive to B_1 and B_0 inhomogeneities because it uses an adiabatic full passage (AFP) pulse for signal inversion; however, because the 3D Cones sequence is not a clinically available sequence (it is primarily available in GE research scanners), the STAIR-Cones sequence is currently limited in its potential for clinical translation.

In this study, we proposed a new clinically translational MWI sequence for whole-brain MWI and quantification, which is a combination of the STAIR technique and echo-planar imaging (EPI) readout. Unlike the research-dedicated Cones sequence, the EPI sequence is a routinely used clinical sequence that is available to all vendors, posing the proposed STAIR-EPI as a technique with greater potential in clinical translation than STAIR-Cones. Moreover, similar to the ViSTa and STAIR-Cones techniques, the proposed STAIR-EPI does not require complicated post-processing such as solving the ill-conditioned problems for those multicompartment modeling techniques (15–17). We investigated the feasibility of the proposed STAIR-EPI technique for the quantification of MWF and compared its values in the lesions and normal-appearing white matter (NAWM) of seven MS patients against the values of NWM of seven healthy volunteers on a clinical 3 T MRI scanner.

2. Materials and methods

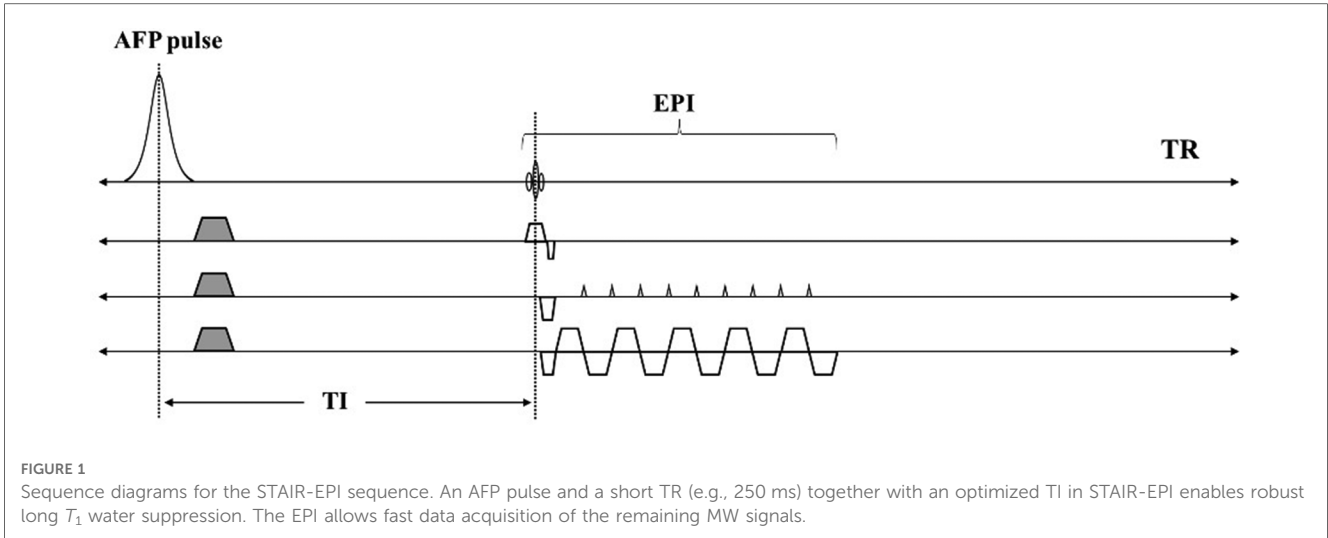
2.1. STAIR-EPI sequence

Figure 1 shows a diagram of the STAIR-EPI sequence. After an AFP pulse and duration of longitudinal magnetization recovery, a blipped multi-shot EPI is used for fast data acquisition. The EPI starts with a 90° radiofrequency (RF) excitation pulse. Inversion time (TI) is determined as the time interval between the center of AFP to the center of the excitation pulse. A short TR between 180 and 300 ms is typically used in the STAIR sequence and, with an appropriate TI (37), signals from long T_1 water components with a broad range of T_1 s (in this case, 600–2,000 ms) can be well suppressed.

The signal equation for the STAIR-EPI sequence is expressed as follows:

$$S_{\text{STAIR}} = M_0(1 - Qe^{-TR/T_1} - (1 - Q)e^{-TI/T_1})e^{-\frac{TR}{T_2}}. \quad (1)$$

$M_0 = [M_0^{\text{MW}}, M_0^L]$ are the longitudinal magnetizations of MW and long T_1 water components in the equilibrium state. $S_{\text{STAIR}} = [S_{\text{STAIR}}^{\text{MW}}, S_{\text{STAIR}}^L]$ are the signal intensities of MW and long T_1 water components in STAIR-EPI imaging. Q represents the inversion efficiency for the AFP pulse with a range of -1 (full inversion) to 1 (no disturbance to the z-magnetization). For long T_1 water components, Q is assumed to be -1. However, for MW with a short T_2^* of 10 ms, Q is set to -0.75 (i.e., $Q_{\text{MW}} = 0.75$) when a relatively long AFP pulse (i.e., 8.64 ms) is utilized for signal inversion based on Bloch simulation (37–40). Our previous numerical simulation demonstrated that a TR



range of [180, 300] ms provides a reasonable contrast-to-noise ratio (CNR) efficiency in STAIR MWI (37). Similar to the STAIR-Cones for MWI, a TR of 250 ms was selected for STAIR-EPI imaging in this study. The corresponding optimal TI (i.e., $TI_{optimal}$) of the STAIR-EPI sequence is determined by minimizing the signals of long T_1 components with a wide range of T_1 values [i.e., (600, 2,000)ms] [see Equation (11) in Ref. (37)]. With the determined $TI_{optimal}$, the MW signal can be expressed as follows:

$$S_{STAIR}^{MW} = M_0^{MW} (1 - Q_{MW} e^{-TR/T_1} - (1 - Q_{MW}) e^{-TI_{optimal}/T_{1,MW}}) e^{-\frac{TE}{T_{2,MW}^*}} \quad (2)$$

$T_{1,MW}$ and $T_{2,MW}^*$ are T_1 and T_2^* of MW respectively. To facilitate the quantification of apparent MWF (aMWF), a proton density-weighted EPI (PD-EPI) sequence is also scanned for total water imaging. The signal equation of the PD-EPI sequence is expressed as follows:

$$S_{PD} = M_0^{total} e^{-\frac{TE}{T_{2,total}^*}} \quad (3)$$

$M_{0,total}$ and $T_{2,total}^*$ are the equilibrium longitudinal magnetization and T_2^* of total water respectively.

aMWF is defined as the PD ratio of MW to total water, and is expressed as follows:

$$aMWF = \frac{M_0^{MW}}{M_0^{total}} \quad (4)$$

With known signal intensities of MW and total water (i.e., S_{STAIR}^{MW} and S_{PD}), the aMWF can be easily computed by the division operation between Equations (2) and (3). The T_1 and T_2^* values of MW ($T_{1,MW}$ and $T_{2,MW}^*$) are set to 220 and 10 ms respectively (16–18, 23, 35, 36). The T_2^* of total water ($T_{2,total}^*$) is set to 60 ms (16, 23).

2.2. In vivo study

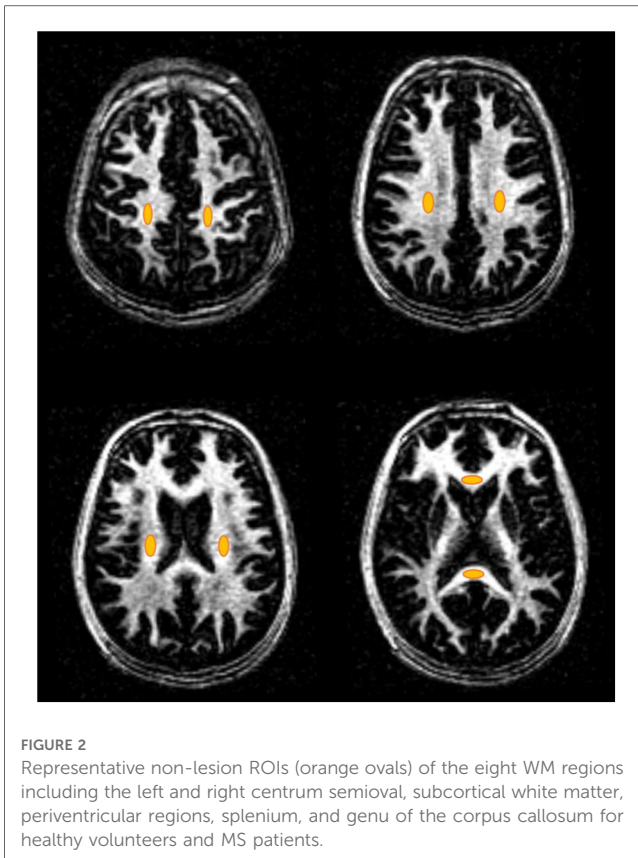
This study was approved by our institutional review board (IRB) and informed consent was obtained from all participants. Seven healthy volunteers (mean age: 39.9 ± 15.9 years, 3 males and 4 females) and seven MS patients (mean age: 53.7 ± 8.7 years, 2 males and 5 females) were recruited and underwent MRI scans. The inclusion criteria for the disease group included a documented diagnosis of MS and age over 18; exclusion criteria included concomitant malignancy and other severe diseases like stroke. The inclusion criteria for healthy volunteers were that participants were in good health and over 18 years old. All individuals with any contraindications for MRI were excluded from study participation.

All participants were scanned on a 3 T clinical MRI scanner (MR750, GE Healthcare Technologies, Milwaukee, WI) and a 12-channel head coil was employed for signal reception.

The sequence parameters of the STAIR-EPI and PD-EPI sequences were as follows: i) STAIR-EPI: field of view (FOV) = $22 \times 22 \text{ cm}^2$, matrix = 128×128 , TR/TI/TE = 250/117/5.5 ms, flip angle (FA) = 90° , number of shots = 8, slice thickness = 5 mm, number of slices = 15, number of excitations (NEX) = 30, and scan time = 15 min; (ii) PD-EPI: FOV = $22 \times 22 \text{ cm}^2$, matrix = 128×128 , TR/TE = 250/5.5 ms, FA = 5° , slice thickness = 5 mm, number of slices = 15, NEX = 10, and scan time = 43s. A clinical T_2 -FLAIR sequence included for diagnosis was scanned with the following parameters: FOV = $25.6 \times 25.6 \times 16.3 \text{ cm}^3$, matrix = $256 \times 256 \times 136$, TR/TI/TE = 7,000/2,028/130 ms, acceleration factor = 4, and scan time = 5.5 min.

2.3. Data analysis

MS lesion regions in MS patients (a total of 66 lesions) and eight non-lesion white matter regions in healthy volunteers (i.e., NWM) and MS patients (i.e., NAWM) were manually drawn for aMWF quantification. The non-lesion regions included the left



and right centrum semioval, subcortical white matter, periventricular regions, splenium, and genu of the corpus callosum (see [Figure 2](#)). Region of interest (ROI) drawings and aMWF calculations were both performed on MATLAB 2022a software (MathWorks Inc., Natick, MA, USA).

A comparison of aMWF measurement was made between NWM in healthy volunteers, NAWM in MS patients, and MS lesions in MS patients. Upon confirming normal distribution through the Kolmogorov-Smirnov test, a one-way ANOVA test was carried out to assess the differences in aMWF among these three groups (i.e., NWM, NAWM, and MS lesions). A *post hoc* test (Games-Howell test) was conducted for paired comparisons between each of the two groups (i.e., NWM vs. NAWM, NWM vs. MS lesions, and NAWM vs. MS lesions). *P* values less than 0.05 indicates statistical significance.

3. Results

[Figure 3](#) shows the representative STAIR-EPI and PD-EPI images as well as corresponding aMWF maps from a 31-year-old male healthy volunteer. Much higher MW signal intensities in the STAIR-EPI images are found in white matter regions than those in grey matter regions. The aMWF maps also demonstrate a higher aMWF in the white matter region than in the grey matter region.

[Figure 4](#) shows representative T_2 -FLAIR, PD-EPI, and STAIR-EPI images as well as aMWF maps from three MS patients. The

hyperintense lesions in T_2 -FLAIR show low signal intensities in the STAIR-EPI images and also have lower aMWF values than NAWM regions, demonstrating a decrease in MW content for these MS lesions.

[Table 1](#) summarizes the mean and standard deviation (SD) values of the aMWF measurements from all participants. The aMWF value of NWM in healthy volunteers is $10 \pm 1.3\%$, while the aMWF values of NAWM and MS lesions in MS patients are $8.6 \pm 1.2\%$ and $3.6 \pm 1.3\%$, respectively. Significant difference is achieved between these three groups ($p < 0.001$).

[Figure 5](#) shows the paired comparison of measured aMWF values on each of the two groups (i.e., NWM vs. NAWM, NWM vs. MS lesions, and NAWM vs. MS lesions). The results indicate a notable distinction of aMWF measurements between MS lesions against both NAWM and NWM ($p < 0.001$). A significant difference in aMWF measurement is also observed between NAWM and NWM ($p < 0.001$). These results demonstrate the feasibility of the STAIR-EPI technique in the detection of demyelination in MS.

4. Discussion

In this study, we developed a new translational STAIR-EPI sequence for selective MWI and aMWF quantification in the whole brain. In MS patients, the hyperintense MS lesions in T_2 -FLAIR showed low signal intensities in the STAIR-EPI images, indicating high sensitivity in the detection of demyelination for the STAIR-EPI technique. Moreover, the measured aMWF values of MS lesions ($3.6 \pm 1.3\%$) and NAWM ($8.6 \pm 1.2\%$) in MS patients were significantly lower than those of NWM ($10 \pm 1.3\%$) in healthy volunteers. This study reveals the effectiveness of the STAIR-EPI technique in detecting myelin loss in both MS lesions and NAWM in MS patients, a capability that could subsequently be applied in clinical MRI scanners from all vendors. The implementation of the proposed STAIR-EPI sequence is relatively easy and requires neither specialized involvement from scanner vendors nor from application specialists.

EPI is one of the fastest MRI sequences and has already made significant contributions to clinical diagnosis and scientific investigation for various parts of the body including the brain, abdomen, and pelvis (41). With single-shot EPI, a complete set of spatial-encoding data can be gathered following a single RF excitation. However, single-shot EPI suffers from strong imaging distortion induced by eddy currents and B_0 inhomogeneity due to the low bandwidth in the phase-encoding direction. Multi-shot EPI strategy mitigates the imaging distortion because of its increased bandwidth in the phase-encoding direction. In this study, the STAIR technique was combined with the multi-shot EPI acquisition scheme to achieve relatively high-quality MWI. The image quality improved with more shots, but more shots also led to increased scan time (42). We found that eight shots provided a reasonable level of image quality within an acceptable 15-minute scan time.

One of the major advantages of the STAIR-EPI technique is its simplicity, given that it requires neither complex sequence

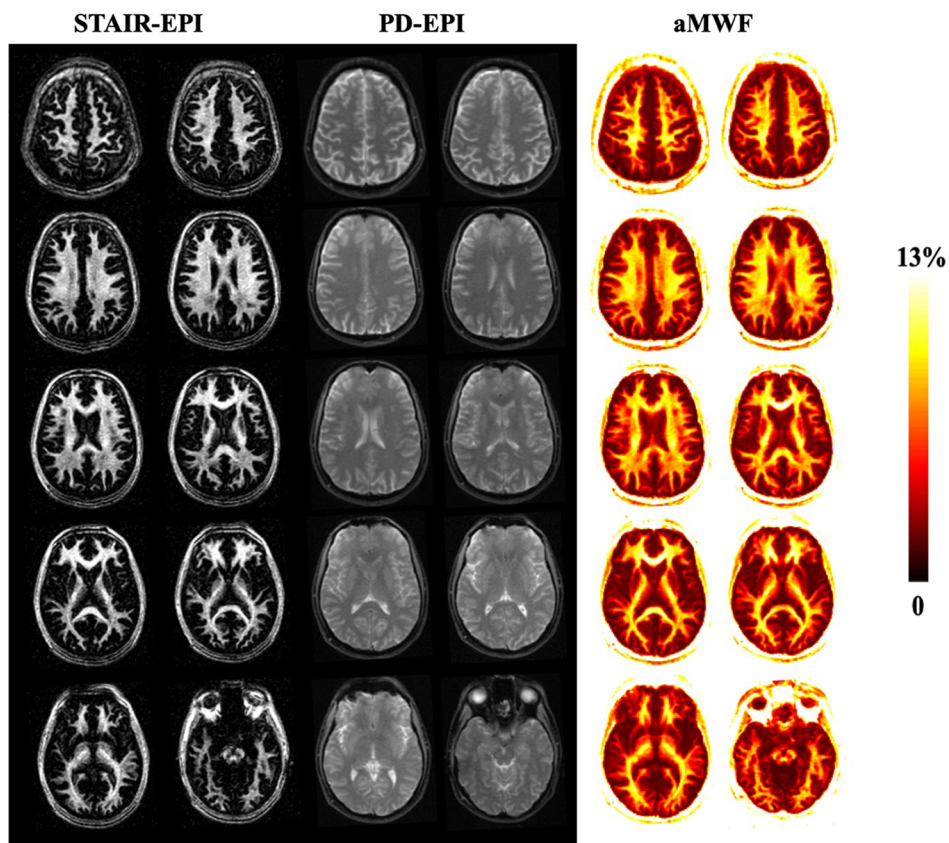


FIGURE 3
 Representative STAIR-EPI (columns 1 and 2) and PD-EPI (columns 3 and 4) images, as well as the corresponding aMWF maps (columns 5 and 6) from a 31-year-old healthy male volunteer. White matter regions have a much higher myelin water content than gray matter regions.

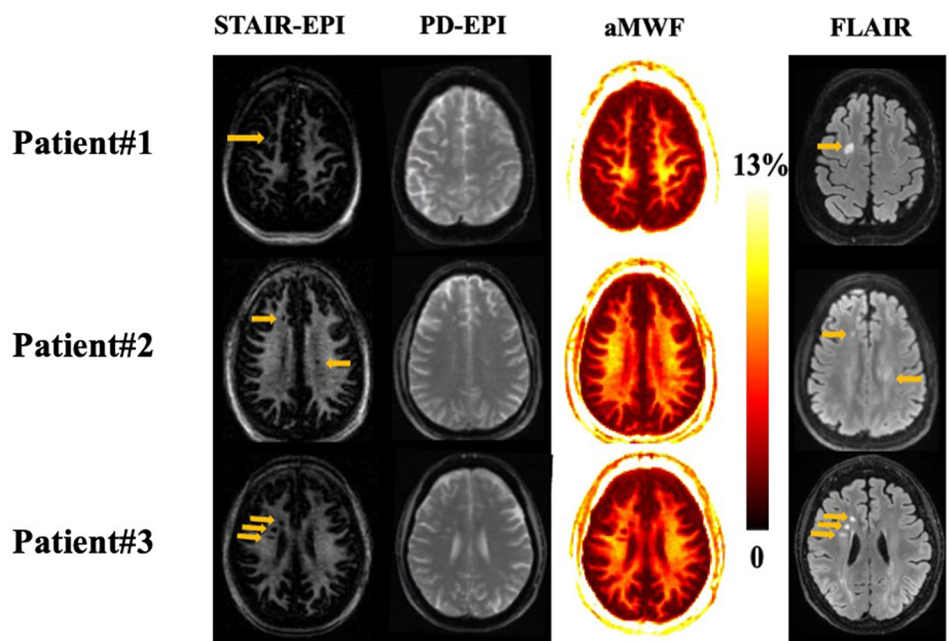
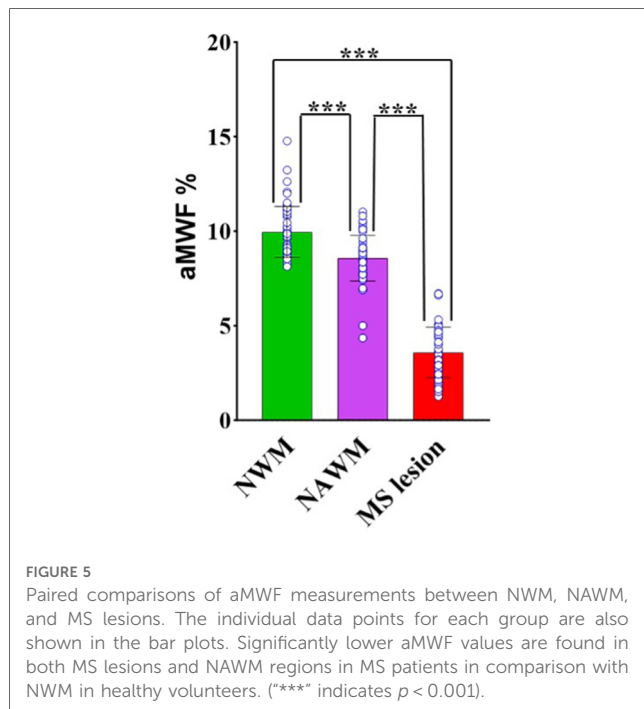


FIGURE 4
 Representative STAIR-EPI (first column), PD-EPI (second column), and aMWF (third column), as well as T_2 -FLAIR (fourth column) from three patients with MS (patient #1 is a 57-year-old female, patient #2 is a 52-year-old male, and patient #3 is a 67-year-old female). Hyperintense lesions detected on T_2 -FLAIR images (arrows) show a signal loss on the corresponding myelin water images and aMWF maps.

TABLE 1 Mean and standard deviation (SD) of aMWF measurements from NWM, NAWM, and MS lesions as well as one-way ANOVA test results for these three groups.

	aMWF	95% CI	P Value (one-way ANOVA test)
	(%, mean \pm STD)		
NWM	9.9 \pm 1.3%	9.6–10.3	<0.001
NAWM	8.5 \pm 1.2%	8.2–8.8	
MS Lesion	3.6 \pm 1.3%	3.3–3.9	

Significant difference is achieved between the three groups ($p < 0.001$). Confidence intervals (CI) at a 95% confidence level provide US with a range of values that is likely to include the true population mean for each group.



implementation nor complicated post-processing in comparison to conventional techniques (24, 28–30, 37). Additionally, the STAIR preparation is relatively insensitive to B_0 and B_1 field inhomogeneities because it uses the AFP pulse for magnetization inversion (43). These benefits make the STAIR-EPI technique well-suited for clinical practice. Both DIR and STAIR are effective techniques for selective imaging of short T_1 MW and signal suppression of long T_1 intracellular and extracellular water in the brain (32, 37). However, the STAIR technique has an improved scan efficiency over the DIR technique because of its much shorter TR.

Previous research on the MWF quantification in NWM has presented a range of values using different methodologies (15–18, 23, 26, 44–49). For example, multicomponent T_2 decay analysis estimated MWFs ranging from 9% to 15.6% (15, 44–48), whereas multicomponent T_2^* decay analysis yielded an MWF range of 6.9% to 14.4% (9, 16, 23, 26, 49). Labadie et al. employed multicomponent T_1 modeling and determined an MWF of 8.3% (18). Ma et al., employing the 3D STAIR-Cones technique, found an MWF value of 9.2% (37). Moreover, a range of MWF values has also been reported for MS lesions in previous MWI studies

(15, 37, 48, 49). The multicomponent T_2 analysis indicated MWFs ranging from 1.7% to 6.4% (15, 48), while a multicomponent T_2^* analysis determined an MWF of $\sim 0\%$ (49). For the most recent STAIR-Cones study, Ma et al. reported an MWF value of 4.5% for MS lesions (37). In this study, the mean MWF values of NWM (i.e., $10 \pm 1.3\%$) and MS lesions (i.e., $3.6 \pm 1.3\%$) are consistent with those reported in previous research.

As reported in previous studies, the multicomponent T_2 relaxometry sequence took between 25 and 38 min to complete (45, 46), whereas the multicomponent T_2^* relaxometry sequence took between 20 and 30 min (16, 26). In comparison, the total scan time for the proposed STAIR-EPI technique is around 16 min, which is relatively shorter than the typical multicomponent T_2 and T_2^* relaxometry techniques.

There were some limitations in this study. First, only seven MS patients were scanned in this technical feasibility study. We plan to recruit more patients to investigate demyelination or remyelination in the future. Second, as proof of concept, a relatively large NEX (i.e., 30) was used in the STAIR-EPI scan to achieve a high SNR performance, significantly prolonging the scan time for whole brain coverage. The scan time could be reduced by using a lower NEX value (e.g., 10 or less). Moreover, the recent development of the denoising technique via deep learning could significantly increase the image SNR, thereby facilitating sufficient SNR improvement with a much reduced NEX (e.g., 5) (50, 51).

5. Conclusion

The STAIR-EPI technique detects demyelination in MS, facilitating easy clinical translation for the whole brain MWI.

Data availability statement

The raw data supporting the conclusions of this article will be made available by the authors, without undue reservation.

Ethics statement

The studies involving humans were approved by University of California San Diego. The studies were conducted in accordance with the local legislation and institutional requirements. Written informed consent for participation in this study was provided by the participants' legal guardians/next of kin.

Author contributions

HS: Formal Analysis, Visualization, Writing – original draft, Data curation, Methodology, Writing – review & editing. DM: Formal Analysis, Visualization, Writing – original draft, Data curation, Methodology, Writing – review & editing. JA: Writing – review & editing, Data curation, Software. SS: Data curation, Writing – review & editing. JL: Data curation, Writing – review

& editing. AS: Data curation, Writing – review & editing. BM: Writing – review & editing, Data curation. YM: Conceptualization, Data curation, Funding acquisition, Investigation, Methodology, Project administration, Resources, Software, Supervision, Writing – review & editing.

Funding

The author(s) declare financial support was received for the research, authorship, and/or publication of this article.

The authors acknowledge grant support from NIH (R01AR079484 and F32AG082458), as well as GE Healthcare. The authors declare that GE Healthcare was not involved in the study design, collection, analysis, interpretation of data, the writing of this article, or the decision to submit it for publication.

References

- Noseworthy JH, Lucchinetti C, Rodriguez M, Weinshenker BG. Multiple sclerosis. *N Engl J Med.* (2000) 343(13):938–52. doi: 10.1056/NEJM200009283431307
- Bean BP. The action potential in mammalian central neurons. *Nat Rev Neurosci.* (2007) 8(6):451–65. doi: 10.1038/nrn2148
- Chabas D, Baranzini SE, Mitchell D, Bernard CC, Rittling SR, Denhardt DT, et al. The influence of the proinflammatory cytokine, osteopontin, on autoimmune demyelinating disease. *Science.* (2001) 294(5547):1731–5. doi: 10.1126/science.1062960
- Steinman MDL. Multiple sclerosis: a coordinated immunological attack against myelin in the central nervous system. *Cell.* (1996) 85(3):299–302. doi: 10.1016/S0092-8674(00)81107-1
- Schmierer K, Wheeler-Kingshott CAM, Tozer DJ, Boulby PA, Parkes HG, Yousry TA, et al. Quantitative magnetic resonance of postmortem multiple sclerosis brain before and after fixation. *Magn Reson Med.* (2008) 59(2):268–77. doi: 10.1002/mrm.21487
- Dousset V, Grossman RI, Ramer KN, Schnall MD, Young LH, Gonzalez-Scarano F, et al. Experimental allergic encephalomyelitis and multiple sclerosis: lesion characterization with magnetization transfer imaging. *Radiology.* (1992) 182(2):483–91. doi: 10.1148/radiology.182.2.1732968
- Newcombe J, Hawkins CP, Henderson CL, Patel HA, Woodroffe MN, Hayes GM, et al. Histopathology of multiple sclerosis lesions detected by magnetic resonance imaging in unfixed postmortem central nervous system tissue. *Brain J Neurol.* (1991) 114(Pt 2):1013–23. doi: 10.1093/brain/114.2.1013
- Filippi M, Rocca MA. MR imaging of multiple sclerosis. *Radiology.* (2011) 259(3):659–81. doi: 10.1148/radiol.11101362
- Alonso-Ortiz E, Levesque IR, Pike GB. MRI-based myelin water imaging: a technical review. *Magn Reson Med.* (2015) 73(1):70–81. doi: 10.1002/mrm.25198
- MacKay AL, Laule C. Magnetic resonance of myelin water: an in vivo marker for myelin. *Brain Plast Amst Neth.* (2016) 2(1):71–91. doi: 10.3233/BPL-160033
- Lee J, Hyun JW, Lee J, Choi EJ, Shin HG, Min K, et al. So you want to image myelin using MRI: an overview and practical guide for myelin water imaging. *J Magn Reson Imaging JMRI.* (2021) 53(2):360–73. doi: 10.1002/jmri.27059
- Piredda GF, Hilbert T, Thiran JP, Kober T. Probing myelin content of the human brain with MRI: a review. *Magn Reson Med.* (2021) 85(2):627–52. doi: 10.1002/mrm.28509
- Does MD. Inferring brain tissue composition and microstructure via MR relaxometry. *NeuroImage.* (2018) 182:136–48. doi: 10.1016/j.neuroimage.2017.12.087
- Möller HE, Bossoni L, Connor JR, Crichton RR, Does MD, Ward RJ, et al. Iron, myelin, and the brain: neuroimaging meets neurobiology. *Trends Neurosci.* (2019) 42(6):384–401. doi: 10.1016/j.tins.2019.03.009
- MacKay A, Whittall K, Adler J, Li D, Paty D, Graeb D. In vivo visualization of myelin water in brain by magnetic resonance. *Magn Reson Med.* (1994) 31(6):673–7. doi: 10.1002/mrm.1910310614
- Du YP, Chu R, Hwang D, Brown MS, Kleinschmidt-DeMasters BK, Singel D, et al. Fast multislice mapping of the myelin water fraction using multicomponent

Conflict of interest

The authors declare that the research was conducted in the absence of any commercial or financial relationships that could be construed as a potential conflict of interest.

Publisher's note

All claims expressed in this article are solely those of the authors and do not necessarily represent those of their affiliated organizations, or those of the publisher, the editors and the reviewers. Any product that may be evaluated in this article, or claim that may be made by its manufacturer, is not guaranteed or endorsed by the publisher.

- analysis of T2* decay at 3T: a preliminary postmortem study. *Magn Reson Med.* (2007) 58(5):865–70. doi: 10.1002/mrm.21409
- Deoni SCL, Rutt BK, Arun T, Pierpaoli C, Jones DK. Gleaning multicomponent T1 and T2 information from steady-state imaging data. *Magn Reson Med.* (2008) 60(6):1372–87. doi: 10.1002/mrm.21704
- Labadie C, Lee JH, Rooney WD, Jarchow S, Aubert-Frécon M, Springer CS Jr, et al. Myelin water mapping by spatially regularized longitudinal relaxographic imaging at high magnetic fields. *Magn Reson Med.* (2014) 71(1):375–87. doi: 10.1002/mrm.24670
- Laule C, Leung E, Lis DKB, Trabulsee AL, Paty DW, MacKay AL, et al. Myelin water imaging in multiple sclerosis: quantitative correlations with histopathology. *Mult Scler Houndmills Basingstoke Engl.* (2006) 12(6):747–53. doi: 10.1177/1352458506070928
- Laule C, Kozlowski P, Leung E, Li DKB, Mackay AL, Moore GRW. Myelin water imaging of multiple sclerosis at 7 T: correlations with histopathology. *NeuroImage.* (2008) 40(4):1575–80. doi: 10.1016/j.neuroimage.2007.12.008
- Laule C, Vavasour IM, Moore GRW, Oger J, Li DKB, Paty DW, et al. Water content and myelin water fraction in multiple sclerosis. A T2 relaxation study. *J Neurol.* (2004) 251(3):284–93. doi: 10.1007/s00415-004-0306-6
- Kolind S, Matthews L, Johansen-Berg H, Leite MI, Williams SCR, Deoni S, et al. Myelin water imaging reflects clinical variability in multiple sclerosis. *NeuroImage.* (2012) 60(1):263–70. doi: 10.1016/j.neuroimage.2011.11.070
- Hwang D, Kim DH, Du YP. In vivo multi-slice mapping of myelin water content using T2* decay. *NeuroImage.* (2010) 52(1):198–204. doi: 10.1016/j.neuroimage.2010.04.023
- Prasloski T, Mädler B, Xiang QS, MacKay A, Jones C. Applications of stimulated echo correction to multicomponent T2 analysis. *Magn Reson Med.* (2012) 67(6):1803–14. doi: 10.1002/mrm.23157
- Lee D, Lee J, Lee J, Nam Y. Single-scan z-shim method for reducing susceptibility artifacts in gradient echo myelin water imaging. *Magn Reson Med.* (2018) 80(3):1101–9. doi: 10.1002/mrm.27127
- Shin HG, Oh SH, Fukunaga M, Nam Y, Lee D, Jung W, et al. Advances in gradient echo myelin water imaging at 3 T and 7 T. *NeuroImage.* (2019) 188:835–44. doi: 10.1016/j.neuroimage.2018.11.040
- Lee J, Choi JY, Shin D, Kim EY, Oh SH, Lee J. Exploring generalization capacity of artificial neural network for myelin water imaging. *Investig Magn Reson Imaging.* (2020) 24(4):207. doi: 10.13104/imri.2020.24.4.207
- Nam Y, Lee J, Hwang D, Kim DH. Improved estimation of myelin water fraction using complex model fitting. *NeuroImage.* (2015) 116:214–21. doi: 10.1016/j.neuroimage.2015.03.081
- Lankford CL, Does MD. On the inherent precision of mcDESPOT. *Magn Reson Med.* (2013) 69(1):127–36. doi: 10.1002/mrm.24241
- Zhang J, Kolind SH, Laule C, MacKay AL. Comparison of myelin water fraction from multiecho T2 decay curve and steady-state methods. *Magn Reson Med.* (2015) 73(1):223–32. doi: 10.1002/mrm.25125
- Deoni SCL, Matthews L, Kolind SH. One component? Two components? Three? The effect of including a nonexchanging “free” water component in multicomponent

- driven equilibrium single pulse observation of T1 and T2. *Magn Reson Med.* (2013) 70(1):147–54. doi: 10.1002/mrm.24429
32. Oh SH, Bilello M, Schindler M, Markowitz CE, Detre JA, Lee J. Direct visualization of short transverse relaxation time component (ViSTa). *NeuroImage.* (2013) 83:485–92. doi: 10.1016/j.neuroimage.2013.06.047
33. Stanisz GJ, Odobina EE, Pun J, Escaravage M, Graham SJ, Bronskill MJ, et al. T1, T2 relaxation and magnetization transfer in tissue at 3 T. *Magn Reson Med.* (2005) 54(3):507–12. doi: 10.1002/mrm.20605
34. Lancaster JL, Andrews T, Hardies LJ, Dodd S, Fox PT. Three-pool model of white matter. *J Magn Reson Imaging JMRI.* (2003) 17(1):1–10. doi: 10.1002/jmri.10230
35. Helms G, Hagberg GE. In vivo quantification of the bound pool T1 in human white matter using the binary spin-bath model of progressive magnetization transfer saturation. *Phys Med Biol.* (2009) 54(23):N529–540. doi: 10.1088/0031-9155/54/23/N01
36. Rioux JA, Levesque IR, Rutt BK. Biexponential longitudinal relaxation in white matter: characterization and impact on T1 mapping with IR-FSE and MP2RAGE. *Magn Reson Med.* (2016) 75(6):2265–77. doi: 10.1002/mrm.25729
37. Ma YJ, Jang H, Lombardi AF, Corey-Bloom J, Bydder GM. Myelin water imaging using a short-TR adiabatic inversion-recovery (STAIR) sequence. *Magn Reson Med.* (2022) 88(3):1156–69. doi: 10.1002/mrm.29287
38. Larson PEZ, Conolly SM, Pauly JM, Nishimura DG. Using adiabatic inversion pulses for long-T2 suppression in ultra-short echo time (UTE) imaging. *Magn Reson Med.* (2007) 58(5):952–61. doi: 10.1002/mrm.21341
39. Horch RA, Gochberg DF, Nyman JS, Does MD. Clinically-compatible MRI strategies for discriminating bound and pore water in cortical bone. *Magn Reson Med.* (2012) 68(6):1774–84. doi: 10.1002/mrm.24186
40. Sussman MS, Pauly JM, Wright GA. Design of practical T2-selective RF excitation (TELEX) pulses. *Magn Reson Med.* (1998) 40(6):890–9. doi: 10.1002/mrm.1910400615
41. Poustchi-Amin M, Mirowitz SA, Brown JJ, McKinsty RC, Li T. Principles and applications of echo-planar imaging: a review for the general radiologist. *Radiogr Rev Publ Radiol Soc N Am Inc.* (2001) 21(3):767–79. doi: 10.1148/radiographics.21.3.g01ma23767
42. An H, Ma X, Pan Z, Guo H, Lee EYP. Qualitative and quantitative comparison of image quality between single-shot echo-planar and interleaved multi-shot echo-planar diffusion-weighted imaging in female pelvis. *Eur Radiol.* (2020) 30(4):1876–84. doi: 10.1007/s00330-019-06491-3
43. Tannús A, Garwood M. Adiabatic pulses. *NMR Biomed.* (1997) 10(8):423–34. doi: 10.1002/(sici)1099-1492(199712)10:8<423::aid-nbm488>3.0.co;2-x
44. Kolind SH, Mädler B, Fischer S, Li DKB, MacKay AL. Myelin water imaging: implementation and development at 3.0 T and comparison to 1.5 T measurements. *Magn Reson Med.* (2009) 62(1):106–15. doi: 10.1002/mrm.21966
45. Whittall KP, MacKay AL, Graeb DA, Nugent RA, Li DK, Paty DW. In vivo measurement of T2 distributions and water contents in normal human brain. *Magn Reson Med.* (1997) 37(1):34–43. doi: 10.1002/mrm.1910370107
46. Nguyen TD, Wisnieff C, Cooper MA, Kumar D, Raj A, Spincemaille P, et al. T2 prep three-dimensional spiral imaging with efficient whole brain coverage for myelin water quantification at 1.5 tesla. *Magn Reson Med.* (2012) 67(3):614–21. doi: 10.1002/mrm.24128
47. Prasloski T, Rauscher A, MacKay AL, Hodgson M, Vavasour IM, Laule C, et al. Rapid whole cerebrum myelin water imaging using a 3D GRASE sequence. *NeuroImage.* (2012) 63(1):533–9. doi: 10.1016/j.neuroimage.2012.06.064
48. Oh J, Han ET, Pelletier D, Nelson SJ. Measurement of in vivo multi-component T2 relaxation times for brain tissue using multi-slice T2 prep at 1.5 and 3 T. *Magn Reson Imaging.* (2006) 24(1):33–43. doi: 10.1016/j.mri.2005.10.016
49. Lenz C, Klarhöfer M, Scheffler K. Feasibility of in vivo myelin water imaging using 3D multigradient-echo pulse sequences. *Magn Reson Med.* (2012) 68(2):523–8. doi: 10.1002/mrm.23241
50. Chen Z, Pawar K, Ekanayake M, Pain C, Zhong S, Egan GF. Deep learning for image enhancement and correction in magnetic resonance imaging—state-of-the-art and challenges. *J Digit Imaging.* (2023) 36(1):204–30. doi: 10.1007/s10278-022-00721-9
51. Tamada D. Review: Noise and artifact reduction for MRI using deep learning. Published online February 28, 2020. doi: 10.48550/arXiv.2002.12889.